Transition period between vegetation growth and senescence controls interannual variability of C fluxes in a Mediterranean reed wetland

P. Serrano-Ortiz[1,2], S. Aranda-Barranco[1], A. López-Ballesteros[3], C. Lopez-Canfin[4], E. P. Sánchez-Cañete[2,5], A. Meijide[6], and A. S. Kowalski[2,5]

[1]Department of Ecology, University of Granada, 18071 Granada, Spain. [2]Andalusian Institute for Earth System Research (CEAMA-IISTA), University of Granada, 18006 Granada, Spain. [3]Department of Botany, School of Natural Sciences, Trinity College Dublin, Dublin, Ireland. [4]Department of Desertification and Geo-Ecology, Experimental Station of Arid Zones (EEZA-CSIC), 04120 La Cañada, Almería, Spain, [5]Department of Applied Physics, University of Granada, 18071 Granada, Spain. [6]Department of Crop Sciences, Division Agronomy, University of Göttingen, 37075 Göttingen, Germany.

Corresponding author: P. Serrano-Ortiz (penelope@ugr.es)

Preprint version. Please cite original version:

Key Points:

- Interannual variability of C fluxes of the Mediterranean wetland mainly depends on the behavior of reed dynamics during the transition to senescence period

- Evapotranspiration of the Mediterranean reed wetland does not present a relevant interannual variability

- The role of the Mediterranean reed wetland in the global warming is determined far more by the CO_2 than the CH_4

Abstract

Wetlands are crucial ecosystems modulating climate change due to their great potential to capture carbon dioxide (CO_2), emit methane (CH_4) and regulate local climate through evapotranspiration (ET). Common reed wetlands are particularly interesting given their high productivity, abundance and highly efficient internal gas-transport mechanism. However, little is known about the interannual behavior and dominant controlling factors of Mediterranean reed wetlands, characterized by seasonal flooding and remarkable weather variability. After 6 years of ecosystem carbon and ET flux measurements by eddy covariance (3 years for CH_4 fluxes), this study shows the functional vulnerability of such wetlands to climate variability, switching between carbon (CO_2+CH_4) sink (660 g CO_2-eeq m^{-2} y^{-1}, in 2014) and source (360 g CO_2-eq m^{-2} y^{-1}, in 2016) in short periods of time. According to our analyses, the great interannual variability appeared to mainly depend on the behavior of reed growth dynamics during the transition to senescence period, what is confirmed through the Enhanced Vegetation Index as a proxy of photosynthetic activity. Additionally, a similar behavior of seasonal and daily patterns of carbon fluxes and ET was found compared with other wetlands under different climates.

1 Introduction

Currently, climate change is one the greatest problems facing humanity and also an outstanding scientific challenge. Atmospheric CO_2 [*Keeling*, 1960] and CH_4 increases (the two most important greenhouse gases after water vapor) are dramatically impacting the Earth's radiation balance, representing the driving force of current and future climate change [*Luo*, 2007]. Therefore, a fundamental understanding of the global carbon cycle is crucial to promote political decisions to increase carbon sequestration in terrestrial ecosystems. In recent decades, the technological development of eddy covariance "flux towers" has enabled continuous, non-destructive, ecosystem-scale measurements of the carbon (CO_2 and CH_4) and evapotranspiration (ET) fluxes from short (half-hour) to long (multi-decadal) records [*Baldocchi*, 2014; *Dabberdt et al.*, 1993]. Continuous long-term CO_2 and evapotranspiration fluxes of several ecosystems types managed differently are currently available thanks to international networks such us FLUXNET [*Baldocchi et al.*, 2001]. However, despite the recent international efforts to quantify CH_4 fluxes globally, such information is still limited, with important sources of uncertainty mostly attributed to emissions from wetlands and other inland waters [*Petrescu et al.*, 2015; *Saunois et al.*, 2016a; *Saunois et al.*, 2016b].

Wetlands, covering between 2% and 6% of the Earth's land surface [*Millennium-Ecosystem-Assessment*, 2005], are crucial ecosystems modulating climate change given their great potential to capture CO_2, to emit CH_4 and to regulate local climate through ET. Such ecosystems are characterized by high production of living biomass and store ca. 25% of the total soil organic carbon pool globally [*Millennium-Ecosystem-Assessment*, 2005]. In parallel however, the high water table creates anaerobic conditions and enhances methanogenic processes, representing 51-82% of the total CH_4 emissions from all global natural sources [*Kirschke et al.*, 2013]. Therefore, the role of wetlands in global warming is determined by the balance between net atmospheric CO_2 uptake and CH_4 release. Additionally, ET influences temperature and humidity in the atmospheric boundary layer, contributing to convective cloud processes and wind convergence patterns [*Arya*, 1988]. Since ET in vegetated wetlands is the

largest consumer of incoming energy [*Raddatz et al.*, 2009], its effect on energy partitioning, boundary-layer conditions and therefore local climate can be very relevant. Consequently, a better understanding of ET processes in such areas is requested [*Moro et al.*, 2004]. Additionally, one of the areas with the greatest uncertainty associated to its global warming contribution lies in the Mediterranean region [*Janssens et al.*, 2003].

Phragmites australis (common reed) is the most widespread and productive wetland plant species [*Clevering and Lissner*, 1999] extending from cold temperate regions to the tropics. In the northern hemisphere, common reed reaches its maximum biomass in summer (July, August and September) with maximum growth rates increasing from north to south in Europe [*Engloner*, 2009]. In particular, Spanish Mediterranean wetlands are frequently fringed by monospecific, dense, vigorous formations of common reed, with a maximum peak of reed growth at the end of June, decreasing abruptly in October with advanced foliar senescence [*Moro et al.*, 2004]. Such growth dynamics determine the strong seasonality of CO_2 and ET fluxes [*Brix et al.*, 2001]. Additionally, reeds are plants with large leaf surface areas and low aerodynamic resistance to transpiration [*Crundwell*, 1986]. Regarding CH_4 fluxes, given the relevant contribution of plant-mediated gas transport to the total CH_4 emission from this type of wetlands, apart from ebullition and diffusion from water [*Anthony and MacIntyre*, 2016], previous studies suggest that the growth dynamics of reeds also drive marked seasonality and diurnal patterns of CH_4 fluxes [*Kim et al.*, 1998; *van den Berg et al.*, 2016].

Despite the relevance of wetlands in the global carbon budget and the abundance of common reed around the world, there are no available studies in Mediterranean reed wetlands where fluxes of CO_2 and CH_4 were measured simultaneously. What is more, to date, few studies have performed simultaneous measurements of CO_2, CH_4 and ET in reed wetlands using eddy covariance [*van den Berg et al.*, 2016; *Zhang et al.*, 2016]. However, given the limited database of such studies (up to 2 years), interannual variability could not be assessed. Additionally, although the growth dynamics of reeds do not vary much across the northern hemisphere [*Engloner*, 2009], it is well known that different climatological conditions may induce great differences in CO_2, CH_4 and ET fluxes while the effect of seasonal flooding, typical of Mediterranean wetlands, is still unknown. Therefore, long-term datasets are crucial to inform management policies leading to conserve and enhance the cooling capacity of these ecosystems in a context of climate change.

The main objectives of this study are to determine (1) diurnal, seasonal and interannual variations in CO_2, CH_4 and ET fluxes based on six years of continuous measurements (three years for CH_4 fluxes); (2) the underlying processes and controlling factors that explain such variability and finally (3) the contribution of carbon (CO_2 and CH_4) exchange from the Mediterranean reed wetland to the global greenhouse gas (GHG) balance. We hypothesized great seasonal variability in CO_2 fluxes and ET following phenological patterns. Similar behavior was expected for CH_4 fluxes, given the strong contribution of plant-mediated gas transport in reeds. However, since the studied wetland is not flooded during most of the growing season, the contribution of CH_4 emissions into the global warming could be negligible. Regarding interannual variability, since respiration and photosynthesis processes in the studied wetland could be temperature- and water- limited respectively, warmer/cooler years or rainy/dry years are expected to largely cause NEE interannual variability. Finally, given the high productivity of reed wetlands, we hypothesized that the studied site acts as a relevant C

sink, similar to temperate forests (C uptake from 100 to 660 g m^{-2} year^{-1} [*Valentini et al.*, 2000]).

2 Material and Methods

2.1 Site description

The wetland is located in *El Padul* in the province Granada, southern Spain, within the Sierra Nevada National Park. The wetland of about 3.3 km^2 lies in the *Lecrín* valley at an elevation of 744 m and is included in the Ramsar Convention for Wetlands. The average air temperature and total precipitation are 16°C and 450 mm, respectively (period 2002-2013; source: Meteorological station RIA-1810 (http://www.juntadeandalucia.es/medioambiente/), and northwesterly winds prevail. The wetland area has been altered over recent decades by drainage for small-scale agriculture, peat extraction, and by eutrophication derived from agricultural activities and waste-water discharge. Peat extraction near the measured area stopped at the beginning of 2012 provoking a continuous increase of the ground water level. A highly variable water table during the annual cycle (from -90 to 90 cm above the surface) is the result of strong seasonal discharge from spring snow melt in the mountains, human intervention (hydric resources management), and the sub-humid warm climate that includes an extended summer dry period. The area selected for the eddy covariance measurements is mainly composed of sand and gravel intercalated with peat [*Ortiz et al.*, 2004]. Plant density, estimated at the end of the growing season of 2013 by counting the number of individuals in 5 plots (0.25m^2) distributed randomly across the eddy covariance area of influence (footprint), was 290±50 individuals m^{-2}. Mean height and stem diameter at the end of the growing season of 2013 were 240±50cm and 0.45±0.09 cm (mean ±SD of 10 individuals for each plot, n = 50), respectively.

2.2 Eddy covariance and environmental measurements

The flux measurements were carried out on an eddy covariance (EC) tower located inside a patch of common reed (37°0'42.26"N, 3°36'20.65"W) with a fetch of around 0.50 km^2 (Figure 1). Fluxes of CO_2, CH_4 and ET (or the latent heat flux, LE) and the sensible heat flux (H) were estimated by using fast-response (10 Hz) instruments mounted atop a tower at 6 m above the ground level. Two Open-path analyzers measured the densities of CO_2 and H_2O (LI-7500; LI-COR Inc., Lincoln, NE, USA), and CH_4 (LI-7700; LI-COR Inc., Lincoln, NE, USA). These instruments were calibrated periodically (at least twice per year; at the beginning and end of the growing season) using an N_2 standard for zero and variable (but known) gas standards as a span (~500 μmol (CO_2) mol^{-1} and ~10 μmol (CH_4) mol^{-1}). Wind vector components and sonic temperature were measured by a sonic anemometer (CSAT-3, Campbell Scientific, Logan, UT, USA). The instrumentation conditions (mainly cleaning lenses) and tower set up was checked on a monthly basis.

Additionally, environmental and soil state variables were measured. Over a representative ground surface, incoming photosynthetic photon flux densities (PPFD) were measured at 5 m above the ground level by quantum sensors (LI-190, Lincoln, NE, USA). Air temperature (T_a) and relative humidity (RH) were measured by a thermohygrometer (HMP 45C, Campbell Scientific, Logan, UT, USA) at 5 m. The ground water level (GWL) was continuously monitored using a piezo-resistive level transmitter (series 26Y, Keller AG für Druckmesstechnik, Switzerland). Net radiation

was measured using a net radiometer (NR Lite, Kipp & Zonen, Delft, Netherlands) located 5 m above the surface. In addition, four heat flux plates (HFP01SC, Hukseflux, Delft, Netherlands) at 8 cm depth, and two pairs of soil temperature probes (TCAV, Campbell Scientific, Logan, UT, USA) at 2 and 6 cm depth were installed parallel to the surface to calculate the soil heat flux (G) as follows:

$$G = G_{8cm} + Q_s + Q_w,$$

$$Q_s = \rho_s (C_s + C_w \theta) \frac{\Delta T}{\Delta t} \Delta z,$$

$$Q_w = \rho_w C_w \frac{\Delta T}{\Delta t} GWL,$$

where Q_s and Q_w are the energy stored in the soil and water column respectively, ρ_s is the soil apparent density (1250 kg m^{-3}), C_s and C_w are the specific heat of dry soil and water respectively (837 J kg^{-1} °C^{-1} and 4182 J kg^{-1} °C^{-1}), θ is the gravimetric humidity of the soil (in kg kg^{-1}), $\Delta T/\Delta t$ is the variation of soil temperature with time (in seconds), Δz is the thickness of the soil layer above the soil heat flux plates (0.08m) and GWL is the ground water level above the surface (in meters) .

Figure 1. Fetch (patch of common reed, delimited by a continuous white line) and crosswind-integrated footprint of the experimental site following Kljun et al. [2004]. The areas within the footprint contributing the most and 50% to measured fluxes are delimited by continuous and dashed lines, respectively, for daytime (black lines) and nighttime (grey lines) periods. Source Google Earth, image: Landsat, imagery date December 14 2015.

A data logger (CR3000, Campbell Scientific, Logan, UT, USA) managed the environmental and soil measurements and recorded 30 min averages. Finally, the Enhanced Vegetation Index (EVI) was used as a measurement of vegetation greenness and phenological activity over the course of this study [*Huete et al.*, 2002]. The EVI data were obtained from a MODIS-Terra sensor available from the Land Product subset tool [*ORNL DAAC,* 2018]. Spatial and temporal resolutions are 250 m and 16-day [MOD13Q1; *Didan* 2015], from the pixel (0.0625 km^2) centered at the EC tower. Daily EVI values were obtained by linear interpolation.

2.3 Flux data processing and quality control

Half-hourly means, variances and covariances following Reynolds decomposition rules were calculated using the *EddyPro 6.2.0* software to obtain half-hourly fluxes. Eddy flux corrections for density perturbations [*Webb et al.*, 1980], two coordinate rotations [*Kowalski et al.*, 1997], block average method for detrending, covariance maximization method for time lags compensation and analytic corrections of high and low pass filtering effects following *Moncrieff* [2014] and [2004] respectively were applied. Tests of stationarity and turbulence development were applied, providing the flag "0" for high quality fluxes (differences <30 % for both tests), "1" for intermediate quality fluxes (differences <30 % for one test) and "2" for poor quality fluxes (differences >30 % for both tests [*Mauder and Foken*, 2004]. Only fluxes with quality 0 and 1 were used for this study. Finally, averaging periods with low turbulence (averaged friction velocity, $u_* < 0.27$ m s^{-1}; [*Papale et al.*, 2006]) were rejected (59% of the total night-time data). The flux crosswind-integrated footprint, estimated according to *Kljun et al.* [2004], is shown in Figure 1. The location of the area within the footprint that contributed the most to the measured turbulent fluxes (x_peak) and the distance from where the footprint contributes 50% to measured fluxes (x_50) are inside the fetch, with an exception for x_50 during night-time periods when the wind comes from the southeast (110°-180°). These fluxes were rejected, representing 3% of the available night-time data.

The energy balance closure (ratio of the sum of sensible and latent turbulent fluxes, H + LE, to the net radiation minus soil heat flux (Rn - G) was 73% ($R^2 = 0.95$; n = 12672). Since the reasons for such imbalance are not yet solved by the scientist community [*Stoy et al.,* 2013],the measured turbulent fluxes presented in this work were not corrected by the energy balance gap. However, notice that the values of our energy balance closure are within the range reported by most FLUXNET sites [*Wilson et al.*, 2002] providing additional information regarding turbulent flux quality [*Moncrieff et al.*, 1997].

3 Data coverage, gap filling for long term integrations, and partitioning

3.1 Carbon dioxide and water vapor fluxes

Over the study period (May 2012 to June 2018), the percentage of rejected CO_2 (and water vapor) fluxes was 54% (44%) due to instrumentation failure, poor quality data, or low turbulence conditions. From these rejected fluxes, 70% (60%) occurred during night-time periods. These gaps were filled using the marginal distribution sampling technique, applied using the available on-line tool (https://www.bgc-jena.mpg.de/bgi/index.php/Services/REddyProcWeb) and based on the replacement of missing values using a time window of several adjacent days (see *Reichstein et al.*

[2005]). The resulting quality of the filled data were mostly quality "1" (most reliable), with only 8% (6%) of filled data with quality "2" (medium) and 1% (1%) with quality "3" (least reliable).

After the gap-filling procedure using the marginal distribution technique, half hourly CO_2 fluxes were partitioned into gross primary production (GPP) and ecosystem respiration (R_{eco}) using the "night-time data-based estimate" (NB; *Reichstein et al.*, [2005]). The NB algorithm models half-hourly R_{eco} as a function of temperature using night-time data (assuming that GPP is zero);

$$R_{eco} = R_{15} \exp\left[E_0 \left(\left| \frac{1}{15 - 46.02} - \frac{1}{T_a - 46.02} \right| \right) \right] \ (1),$$

where R_{eco} is the ecosystem respiration (μmol C m^{-2} s^{-1}), R_{15} the base respiration at 15°C (μmol C m^{-2} s^{-1}), E_0 the temperature sensitivity (°C) and T_a the air temperature (°C). This relationship is extrapolated to daytime and the difference between the modeled R_{eco} and measured CO_2 fluxes yields the estimated GPP. The quality of the NB algorithm to model R_{eco} was tested by plotting measured R_{eco} (NEE at night) *vs*. the calculated R_{eco} for the whole measured period (Figure 2; slope=0.943±0.006, R^2=0.75, n=8729).
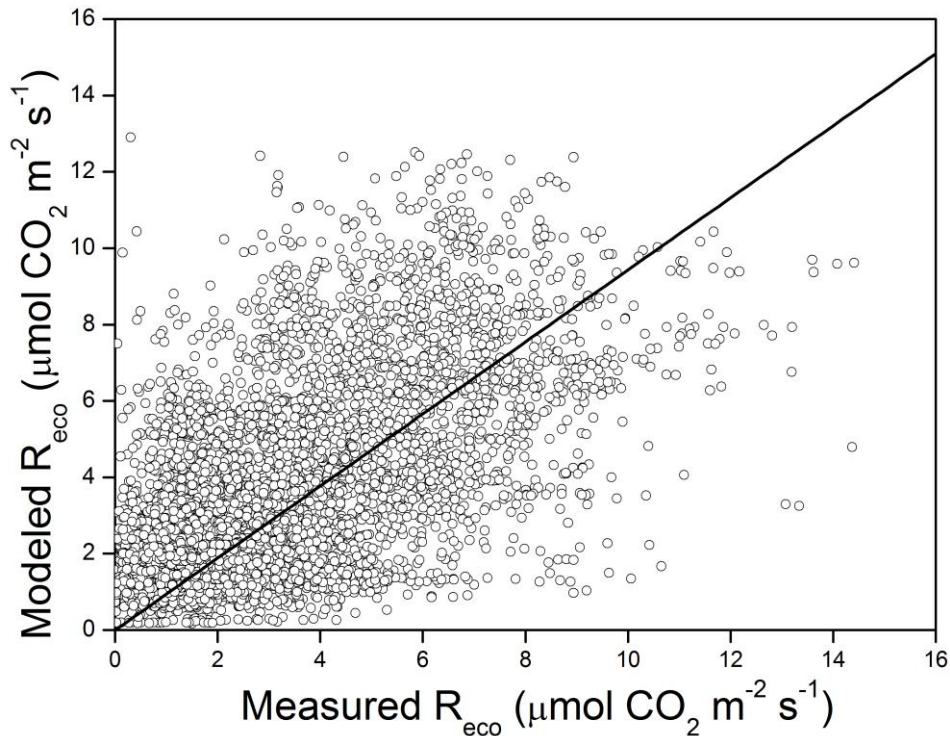

Figure 2. Measured half hourly values of ecosystem respiration (R_{eco}; nightime net ecosystem CO_2 fluxes) vs. modeled R_{eco}.

Since the use of marginal distribution sampling technique for filling gaps can be controversial when it is used to fill continuous days without NEE or ET values, days with more than 75% of absent data were filled using multiple linear regression between daily fluxes and their controlling factors (MLR models; see section 3.3). Uncertainty estimates on NEE and ET balances introduced by the gap-filling process were calculated using the variance of the gap-filled data, which was calculated by introducing

artificial gaps and repeating the standard gap-filling procedure to obtain the variance of each half hourly datapoint. To be conservative with our estimations of annual balances, we estimated their errors as twice the standard deviation of sums of the variances of each half hourly datapoint and the standard deviation of the modeled daily fluxes (whose days with more than 75% of absent half hourly data).

3.2 Methane fluxes

Over the study period (January 2014 to June 2017), the percentage of missing (or rejected) CH_4 flux measurements was 67% mainly due to problems with the data storage system and instrumentation failure. Of these rejected fluxes, 62% occurred during nighttime periods. Given the existence of long data gaps and some periods with lower data coverage (Figure 3), the marginal distribution sampling technique did not allow for seasonal and annual integrations. Instead, we use a machine learning technique (R^2=0.49; RMSE = 0.04 μmol CH_4 m^{-2} s^{-1}). This technique was applied using the *Matlab* software (version R2017a). This method is a type of ensemble decision tree called "Bagging Regression Tree" that uses several decision trees instead of just one to improve the algorithm response; the bagging process is based on generating multiple versions of a predictor to construct a stronger aggregated predictor [*Breiman*, 1996; 2001]. Uncertainty estimates on annual CH_4 emissions introduced by the gap-filling process were calculated using the variance of the gap-filled data, which was calculated by introducing artificial gaps and repeating the standard gap-filling procedure to obtain the variance for each datapoint. Twice the sum of the variance of each half hourly datapoint for each year was taken as the error of our annual balances. The contribution of CH_4 fluxes to global warming was calculated using the most recent global warming potential (GWP) for a 100-year time horizon, not considering climate-carbon feedbacks [*IPCC*, 2013], multiplying the annual CH_4 emission by 28.
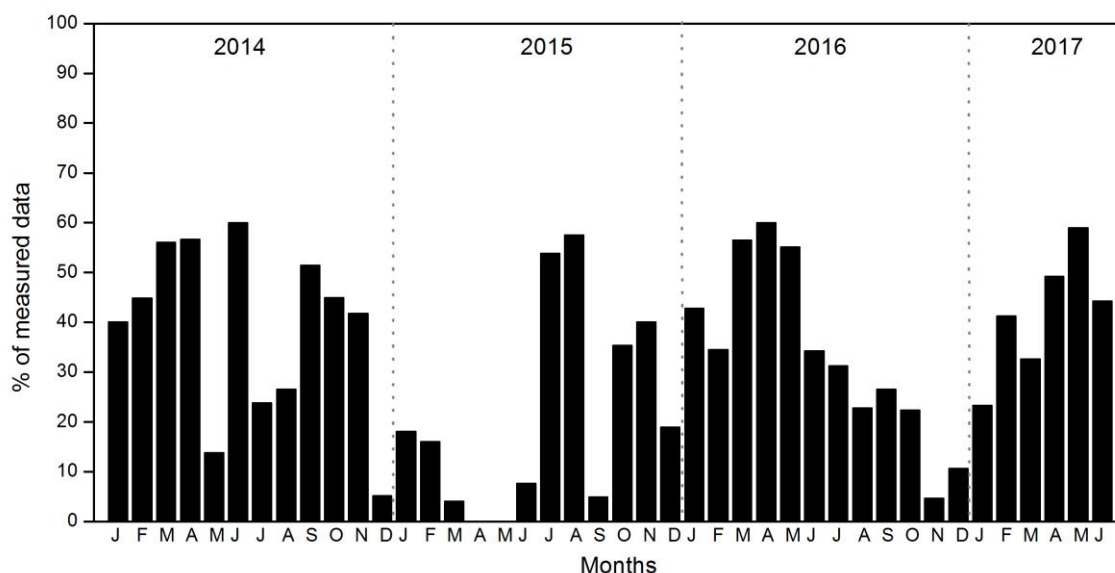

Figure 3. Percentage of measured CH_4 fluxes per month from January 2014 to June 2017. Each column represents (in %) the amount of half hourly data that were measured related to the total half hourly data that potentially can be measured each month.

Water vapor, CO_2 and CH_4 flux analysis at half hourly scales was done using only measured fluxes (data quality flags 0 and 1), whereas for analyses at daily, seasonal or annual scales filled data were also used.

3.3 Statistical analysis

To understand the processes behind the fluxes and explain their variability, we identified the main controlling factors of ET, R_{eco}, GPP, NEE and CH_4 fluxes using statistical modeling. All analyses were done with R software v. 3.5.3 [*R Core Team*, 2019]. In order to avoid issues of collinearity (which is known to produce unstable model parametrization and hence, uninterpretable coefficients), redundant highly correlated variables were excluded from the modeling process based on a preliminary data exploration by principal component analysis. The set of potential predictors remaining to explain our response variables was a compound of ground water level (GWL), enhanced vegetation index (EVI), photosynthetic photon flux density (PPFD), vapor pressure deficit (VPD) and soil temperature (T_s).

To build multiple linear regression models for daily averages of fluxes, the potential predictors (controlling factors) were centered and scaled to zero mean and unit variance in order to generate comparable regression coefficients (because variables had different units). The protocol of *Zuur et al.* [2009] was used to model each response variable. During comparison of models, the best model was always retained as that which minimized the Akaike information criterion (AIC) or improved residual structure. First, a generalized least squares (GLS) linear model was fit with the *gls* function of *Pinheiro and Bates* [2000] which enables to model heteroscedastic and correlated errors. The validity of model assumptions on residuals was inspected: (i) normality; tests for normality become sensitive to even small departures from the initial assumption when the number of observations is large, therefore inspection of the distribution of residuals was preferred, (ii) homoscedasticity; by extension, homoscedasticity tests generally require normality, therefore visualizing the spread of residuals against fitted values was preferred to assess this, and (iii) independence in time. The auto-correlation function (ACF) was plotted to check if autocorrelation differed significantly (risk $\alpha = 0.05$) from zero at different time lags. All these assumptions were initially violated in all models. Therefore, the serial correlation was modeled with an autoregressive-moving-average process (ARMA(p, q), with p and q the orders of the autoregressive and moving-average parts, respectively). To solve heteroscedasticity problems, the residual variance was modeled as inversely proportional to a covariate (VPD for all models except NEE model for which EVI was used instead) and allowing a different residual spread per year. To ensure normality, a power transform was applied on the response variables (Yeo-Johnson transformation for all variables except R_{eco} for which a Box–Cox transformation was used instead). Once all model assumptions were met, a backward variable selection was carried out using the *t-statistic* as the selection criterion, until all terms were significant at the 1% level. The degree of collinearity of the final model was assessed with the variance inflation factor (VIF), ensuring that it was below 10 to validate the model [*Chatterjee and Hadi*, 2012], and Efron´s R² was calculated from the final model fit after back-transforming the predicted response.

Simple linear regression models of response variables were also fitted on annual averages of fluxes. For this purpose, three variables were added to the initial set of potential predictors: rain, length of C uptake and duration of GWL below surface. Since few observations were available, these models were very sensitive to collinearity.

Hence, only one predictor was included in each model, selected as the one producing a significant or almost significant Pearson coefficient of correlation with the response variable. Assumptions on model residuals were checked with statistical tests: the Durbin-Watson´s, Breusch-Pagan´s and Shapiro-Wilk´s tests were used to assess independence, homoscedasticity and normality, respectively. For these annual models, the significance level was set to 5%.

4 Results

4.1 Meteorological conditions and phenology

The studied reed wetland presents strong seasonal variations in meteorological conditions and phenology throughout the study period (Figure 4). Air temperature (T_a) and precipitation present asyncronous patterns with the warmest daily T_a of 26±1°C in July-August, coinciding with absence of precipitation and the lowest ground water level value (GWL) below the surface (-88±11cm). On the other hand, the coldest T_a of 6±1°C registered in December-February coincides with more frequent precipitation events and maximum GWL (34±7cm). Likewise, T_a, VPD showed maximum and minimum values in July-August and December-February, respectively (Figure 4). The EVI shows maximum values in June-August (0.62±0.06) and minimum values in November-January (0.14). Regarding interannual variability, the warmest and the coldest years were 2014 (17.3°C) and 2013 (16.2°C) respectively, with 0.3 degrees higher and 0.8 degrees lower than the average T_a over the study period (17±5 °C), respectively.
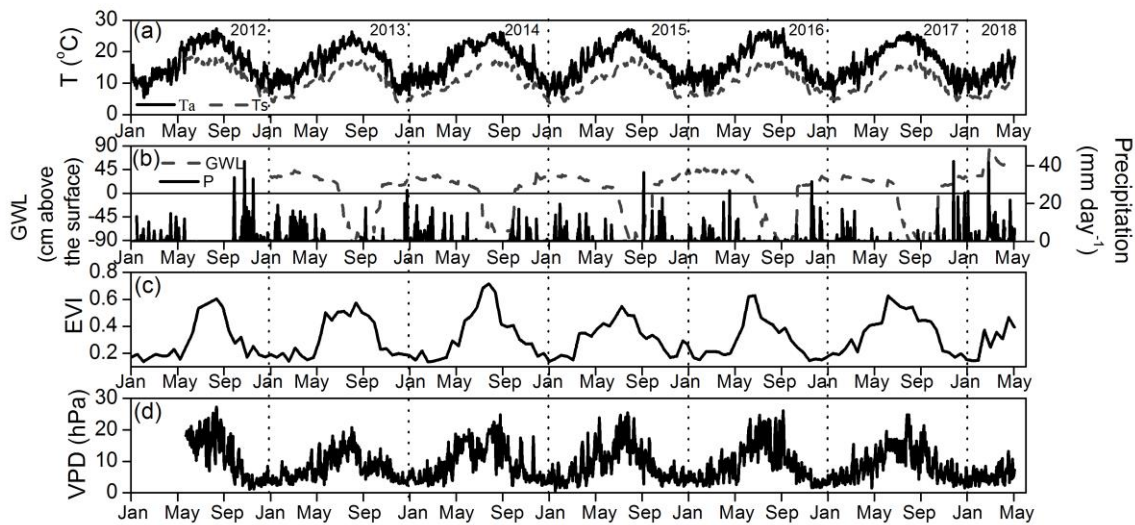

Figure 4. Daily values of (a) air and soil temperature (T_a and T_s), (b) ground water level (GWL) and precipitation, (c) enhanced vegetation index (EVI) and (d) vapor pressure deficit (VPD), in the study period (from May 2012 to June 2018)

4.2 Seasonal and daily patterns

Carbon fluxes and evapotranspiration (ET) present strong seasonal variations throughout the study period (Figure 5). Fluxes of CO_2 and ET have similar but opposite patterns. Maximum values of CO_2 uptake and ET occurred in June and August respectively reaching 8 g C m^{-2} d^{-1} (in 2015) and 9 mm d^{-1} (in 2017), respectively. Maximum daily values of CO_2 emissions up to 6 g C m^{-2} d^{-1} occurred in September 2012 and minimum ET corresponded to null values in January 2014 and 2015. Net CO_2 uptake spanned from June to August and net emission occurred from October to April,

11

coinciding with ET near zero. Similarly, R_{eco} and GPP varied by month (Figure 5). Maximum daily averages of R_{eco} were reached in August-September (8 ± 1 g C m^{-2} d^{-1}), those of GPP occurred in June-July (12 ± 2 ge C m^{-2} d^{-1}), and practically null R_{eco} and GPP occurred in December-January (0.8 ± 0.1 and 0.0 ± 0.1 g C m^{-2} d^{-1}, respectively). By contrast, fluxes of CH_4 followed a different pattern, with maximum emissions in May, (daily averages of up to 110 mg C m^{-2} d^{-1}) and few loose days of September (around 100 mg C m^{-2} d^{-1}) (Figure 5) and near zero emissions in January.
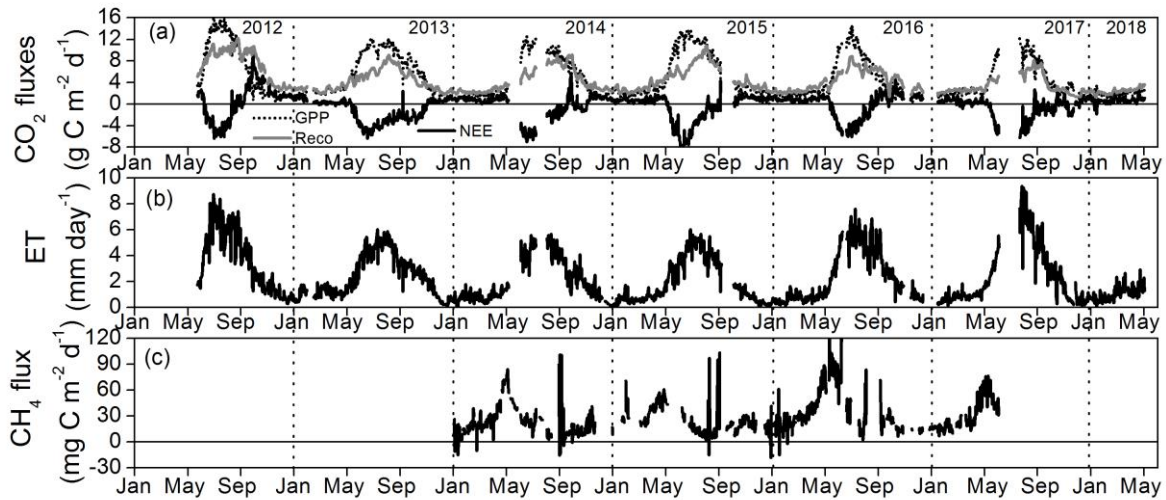

Figure 5. Daily values of (a) CO_2 fluxes (net ecosystem CO_2 exchange (NEE), gross primary production (GPP) and ecosystem respiration (R_{eco})), (b) evapotranspiration (ET) and (c) CH_4 fluxes over the study period (from May 2012 to April 2018). Days with less than 25% of data are not represented.

Different phenological periods were defined based on daily patterns of CO_2 fluxes and ET according to reed phenology: Senescence (from January 1 to May 14 and from November 15 to December 31), Growth (from May 15 to July 31) and Transition (to senescence) (from August 1 to 14 November) periods. Despite differences in magnitude depending on the growth stage, single valley-peak patterns of CO_2 fluxes and ET were mostly observed for all periods, with peak values at noon showing a symmetric pattern (Figure 6). During daytime, the studied wetland acted as a net CO_2 sink for the transition and the growth periods since GPP exceeded R_{eco}. However, for the senescence period, it was CO_2 neutral. At night when photosynthesis vanishes the studied site emitted CO_2 to the atmosphere for all periods. By integrating the averaged values of the diurnal trends of CO_2 fluxes (Figure 6), the daily cumulative fluxes of CO_2 in *Padul* were 1 ± 1, -5 ± 4, and 1 ± 4 gC m^{-2} day^{-1} for the senescence, growth and transition periods respectively. Substantial ET occurred for all periods, with daily averaged values of 1 ± 1, 4 ± 2 and 3 ± 2 mm day^{-1} respectively for each period (senescence, growth and transition). Regarding CH_4 diurnal trends, no differences in the diurnal trends were found for the different phenological periods, except comparing the early growth season (May) with the rest of the year. The highest emission during the early growth period occurred around 10:00 GMT, with peaks of 0.14 ± 0.06 µmol m^{-2} s^{-1}, showing an asymmetric pattern. During night-time, CH_4 emissions decreased in both periods presenting similar values of around 0.01 µmol m^{-2} s^{-1} (Figure 6c). The daily averaged emission of CH_4 in *Padul* was 0.07 ± 0.05 and 0.03 ± 0.05 g C m^{-2} day^{-1} during the early growth and the rest of the period, respectively.
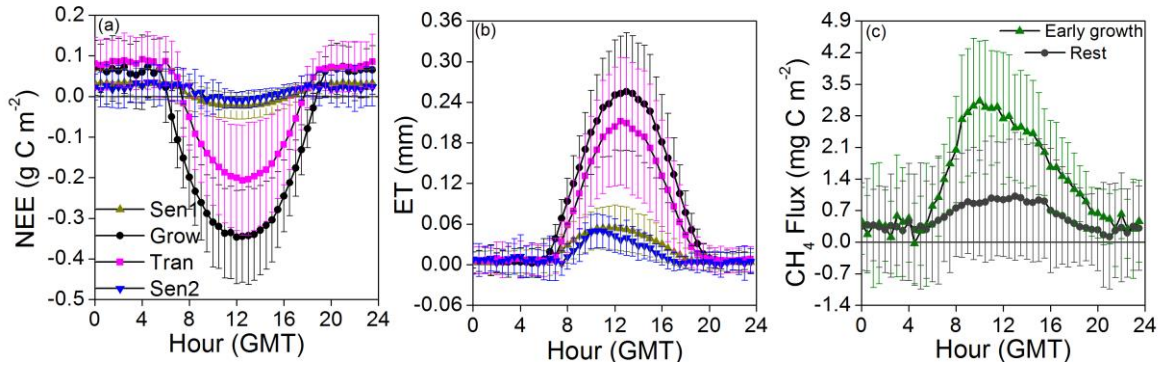
12

Figure 6. Diurnal cycles of net ecosystem carbon exchange (NEE), evapotranspiration (ET) and CH_4 flux for the different growth periods [Senescence "Sen1" from January 1 to May 14 and "Sen2" from November 15 to December 31), Growth (from May 15 to July 31) and Transition (from August 1 to 14 November)]. For CH_4 flux, the periods "Early growth" (May) and the rest of the year "Rest" were presented. Only measured data for the whole studied period were used.

4.3 Annual budgets and contribution of the different phenological periods

The Mediterranean reed wetland acted as a C sink, showing large interannual variability, and absorbing from 10 ± 20 (in 2016) to 410 ± 30 (in 2017) $gC\text{-}CO_2$ m^{-2} y^{-1} (Table 1) over the study period. Notice that an extremely low value of NEE was observed for the reed wetland in 2016 (Table 1, asterisk). That year presented fewer days of net C uptake (92 days), and lower mean annual EVI values (0.29) compared to other years, GPP was very low (1140 g C m^{-2}) whereas R_{eco} was near the annual average, so that the site was more or less C neutral (NEE= -10 g C m^{-2}); additionally, annual CH_4 emissions were the highest for this year. By contrast, in 2017 R_{eco} was very low (961 gC m^{-2}) coinciding with the lowest values of annual mean T_s and GWL. For 2015, R_{eco} was the highest (1366 gC m^{-2}).

Table 1. Annual cumulative fluxes (± uncertainty estimates introduced by the gap-filling process) and annual averaged values of the expected controlling factors.

	ET (mm)	GPP (gC m^{-2})	R_{eco} (gC m^{-2})	NEE (gC m^{-2})	CH_4 flux (gC m^{-2})	EVI	PPFD (μmol m^{-2} s^{-1})	VPD (hPa)	T_a (ºC)	T_s (ºC)	Rain (mm)	Length of C uptake (days)	GWL (cm)	GWL below surface (days)
2013	840±3	1557	1158	-400±10		0.31	396.6	8.0*	16.2*	10.3	438*	175	0	108
2014	802±3	1488	1236	-260±30	8.8±1.2	0.33	396.6	9.6*	17.3	10.8	322	170	0	91*
2015	772±3	1574	1366*	-200±20	8.8±1.3	0.32	385.2	9.0	17.0	10.5	354	121	2	93
2016	833±3	1140*	1135	-10±20*	12.4±1.6*	0.29*	386.2	9.0	17.0	10.7	348	92*	1	112
2017	918±7	1371	961*	-410±30		0.36*	397.8	9.1	17.0	10.1*	274	155	-5	109

Note. Evapotranspiration (ET); growth primary production (GPP); ecosystem respiration (R_{eco}); net ecosystem exchange (NEE); enhanced vegetation index (EVI); photosynthetic photon flux density (PPFD); vapor pressure deficit (VPD); air temperature (T_s); soil temperature (T_s); the number of days of C uptake per year (length of C uptake); ground water level (GWL); the number of days with water table level below the surface per year (GWL below surface).
* Values outside the range "annual averages ± standard deviation"

Each phenological period contributed to the annual NEE in different ways (C sinks or sources) and with different intensities. During senescent periods, the wetland acted as net C source for all years, emitting an average of 130 ± 40 gC (CO_2) m^{-2} y^{-1} (Figure 7a) at a more or less constant rate over the years (Figure 8a). During this period,

13

R_{eco} exceeded GPP by ~120 g (CO_2) m^{-2}; Figure 7a). Similarly, during the growth period the studied wetland acted as net C sink, absorbing an average of 330±30 gC (CO_2) m^{-2} y^{-1} (Figure 7a) at a more or less constant rate over the years (Figure 8a). During this period, GPP almost double R_{eco} (GPP ~680±60 gC m^{-2}; R_{eco} ~370±40 gC m^{-2}; Figure 7a). By contrast, during the transition period, the reed wetland presented the greatest variability among years (averaged NEE$_{transition}$= -56±120 gC (CO_2) m^{-2}; Figure 7a), acting as a large net carbon sink in 2013 and 2017 or as a great and moderate net CO_2 source in 2016 and 2015, respectively (Figure 8a).

By contrast, annual ET did not present a remarkable interannual variability, with values ranging from 918±7 (in 2017) to 772±3 (in 2015) mm (Table 1). Similar ET rates were measured during senescence and growth periods for all years, with total ET of 150±15mm and 350±40mm for each period, respectively (Figure 7b). During the transition period, the greatest and lowest increase in ET occurred in 2017 and 2015 respectively, coinciding with the highest and the lowest annual values of ET (Figure 8b). Similarly to NEE, the total amount of ET for this period presented the greatest variability among years (ET$_{transition}$= 340±60mm; Figure 7b)

Regarding CH$_4$, the studied reed wetland was a slight annual source of CH$_4$ emitting around 9 g C-CH$_4$ m^{-2} in 2014 and 2015, and around 12 g C-CH$_4$ m^{-2} in 2016 (Table 1). CH4 emissions occured at a more or less constant rate over the years (Figure 8c), with the exception around May and June, where the highest emissions were measured in 2016. Therefore, the phenological period that most contributed to the annual CH$_4$ budget was the Senescence1 (the longest period; Figure 7c).
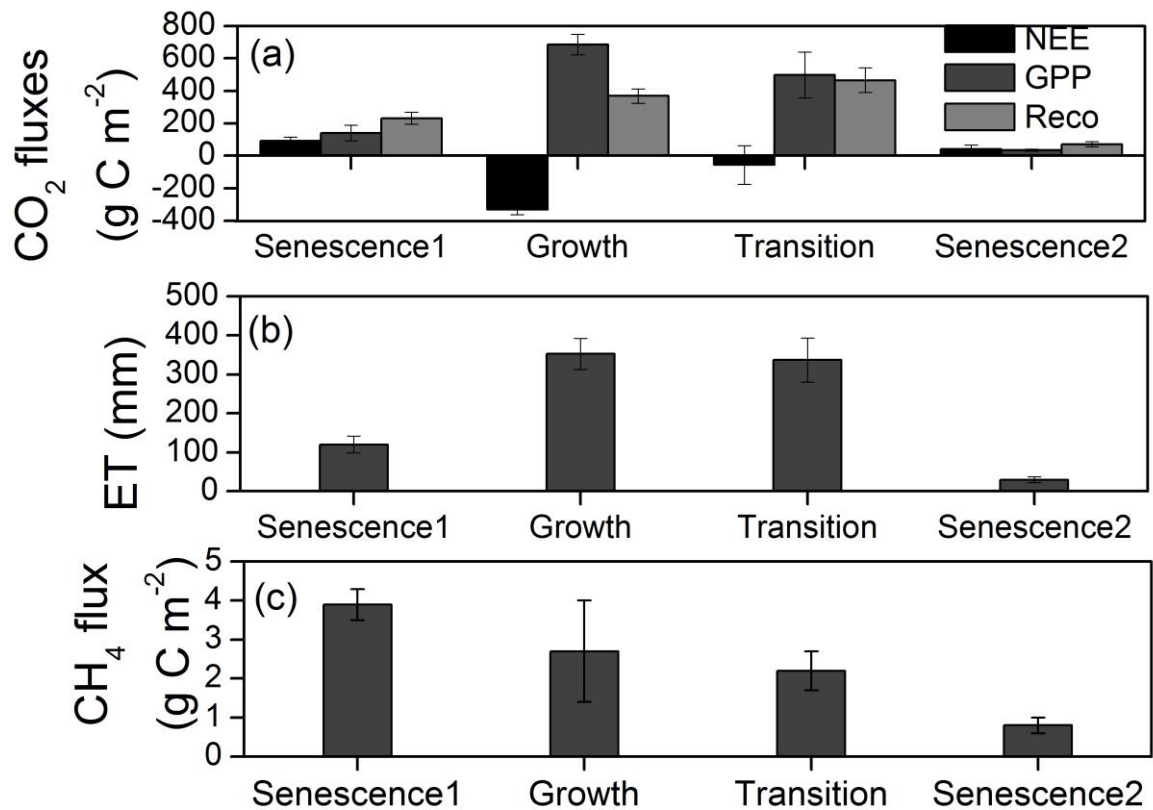

Figure 7. Mean annual (± standard deviation) values of (a) Net Ecosystem C (CO_2) Exchange (NEE), Gross Primary Production (GPP), Ecosystem Respiration (R_{eco}) (b) Evapotranspiration (ET) and (c) CH$_4$ fluxes for the different growth periods (Senescence1, Growth, Transition, Senescence2) from 2013 to 2017 (from 2014 to 2016 for CH$_4$ fluxes).

Finally, taking into account both CO_2 and CH_4 gases, the annual budget of CO_2 equivalents in the Mediterranean reed wetland largely varied between the studied years. In 2014 and 2015 the wetland acted as CO_2 sink (-660±150 and -440±110 g CO_2-eq m^{-2} respectively), whereas in 2016, coinciding with the minimum values of annual net CO_2 uptake and the maximum values of annual CH_4 emissions, the site acted as a source (360±120 gCO_2-eq m^{-2}).
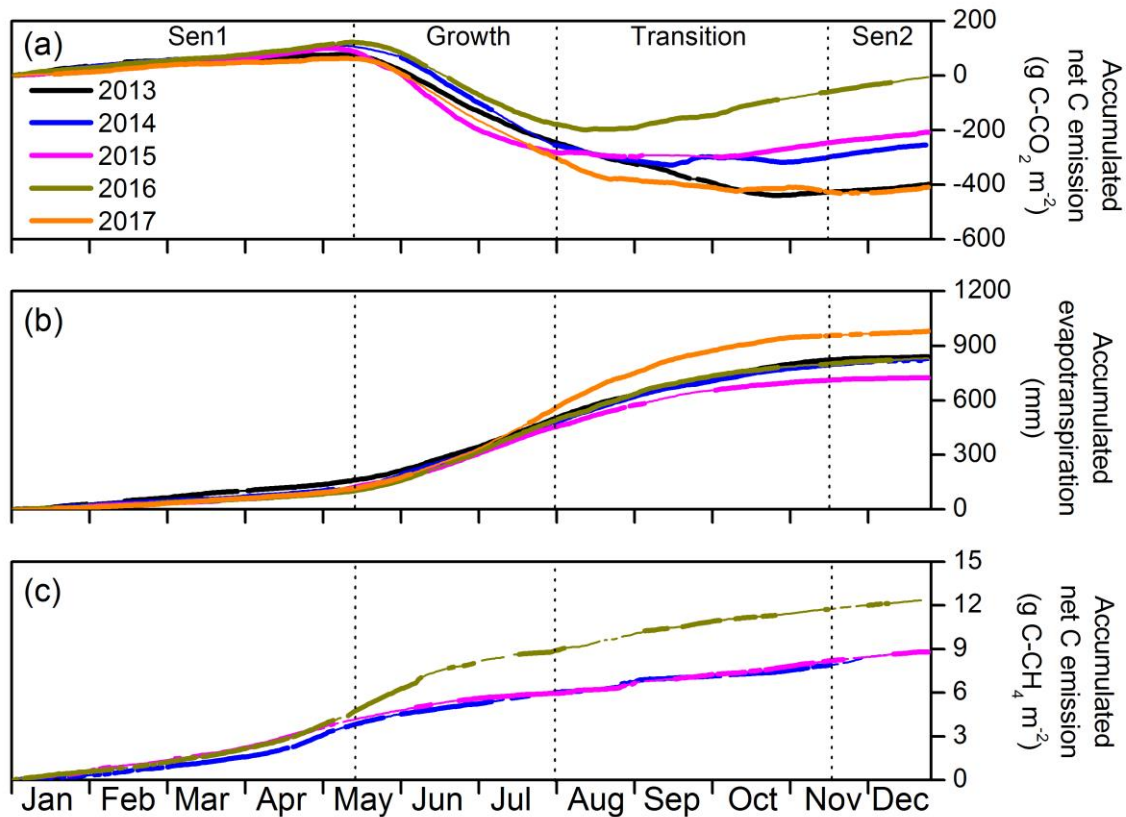

Figure 8. Annual accumulated carbon [(a) for CO_2 and (c) for CH_4] emission and (b) ET in Padul for 2013 to 2017. Dotted lines denote the limits of each growth period (Senescence-Sen1 and Sen2-, Growth and Transition). Fine segments correspond to filled complete days using the non-linear regression models (R_{eco}_NL-GPP_NL) for NEE, the multiple linear regression model for ET and the machine learning technique for CH_4 fluxes.

4.4 Controlling factors affecting the seasonal and interannual variability of carbon and ET fluxes

In order to explain the interannual variability observed for each flux, we selected and fitted multiple linear regression models for daily average values and simple linear regression models for annual averages values. All assumptions of the retained models were acceptable and the VIFs of the selected multivariable models were well below 10 (ranging from 2.5 in the NEE model to 6 in the CH_4 flux model), indicating no collinearity issues.

The summary of multiple linear regression (MLR) models fitted on daily average values of ET, R_{eco}, GPP, NEE and CH_4 fluxes is shown in Table 2. Despite the MLR model for ET included several explanatory variables, T_s by itself had the largest effect size (as indicated by the highest regression coefficient) and explained most of the variation in ET and R_{eco} in the form of a positive correlation. In contrast, GPP was best

explained by a combination of T_s and EVI (Table 2). Although EVI had a larger effect size, T_s contributed likewise substantially to explaining the variations in GPP through positive correlations. The proposed MLR models predicted quite well daily variations and, therefore, seasonal patterns and interannual variability of ET, GPP and R_{eco} (Figure 9), with few exceptions, such as the extraordinarily high ET values measured during July and August in 2017 (Figure 9a) and the high values of GPP in May-July of 2015 (Figure 9b). Regarding NEE, the main explanatory variable was PPFD (Table 2). However the lower goodness of the fit ($R^2 < 0.5$) caused the MLR model to fail at predicting NEE, especially the very variable daily net CO_2 emission/assimilation measured during the transition period (August, September and October) for most of the years (Figure 7d). However, when NEE was modeled as modeled R_{eco} minus modeled GPP, the behavior of NEE during the transition period was better predicted, with an exception in 2015 (Figure 7d). Finally, the MLR model for daily averages of CH_4 fluxes, presented a very low R^2 and therefore, variations in the CH_4 emissions were not well predicted, especially the highest emissions in May.

Table 2. Summary of multiple linear regression models fitted on daily average values of water/carbon fluxes.

Response variable	Explanatory variables	β	SE	p-value	Efron´s R^2
ET	(Intercept)	0.8579	0.0087	<0.0001	
	EVI	0.0643	0.0113	<0.0001	
	PPFD	0.0732	0.0052	<0.0001	0.82
	VPD	0.0663	0.0049	<0.0001	
	Ts	0.1371	0.0119	<0.0001	
R_{eco}	(Intercept)	0.9885	0.0091	<0.0001	
	GWL	-0.0616	0.0117	<0.0001	
	EVI	0.1404	0.0135	<0.0001	0.83
	VPD	0.0998	0.0048	<0.0001	
	Ts	0.3775	0.0175	<0.0001	
GPP	(Intercept)	1.0642	0.0132	<0.0001	
	EVI	0.2224	0.0180	<0.0001	
	PPFD	0.1371	0.0081	<0.0001	0.76
	VPD	0.0388	0.0077	<0.0001	
	Ts	0.1692	0.0195	<0.0001	
NEE	(Intercept)	-0.0935	0.1287	0.47	
	EVI	-0.4002	0.0531	<0.0001	0.45
	PPFD	-0.5897	0.0264	<0.0001	
	VPD	0.2300	0.0245	<0.0001	
CH_4	(Intercept)	0.0173	0.0007	<0.0001	
	GWL	0.0037	0.0007	<0.0001	
	EVI	-0.0032	0.0009	0.0004	0.14
	PPFD	0.0017	0.0004	0.0002	
	VPD	0.0018	0.0004	<0.0001	
	Tsoil	0.0033	0.0011	0.002	

Note. Evapotranspiration (ET); ecosystem respiration (R_{eco}); growth primary production (GPP); net ecosystem exchange (NEE); soil temperature (T_s); enhanced vegetation index (EVI); ground water level (GWL); vapor pressure deficit (VPD); photosynthetic photon flux density (PPFD); linear regression coefficient (β); standard error of β (SE); the proportion of explained variance (Efrons's R^2). Shadow lines highlight the main explanatory variables for each corresponding fluxes. (based on β values). Models were fitted by generalized least squares using power transformed response variables and standardized (centered and scaled to zero mean and unit variance) explanatory variables. Results are based on $n = 1954$ observations except for CH_4 flux model which is based on $n = 1096$ observations.
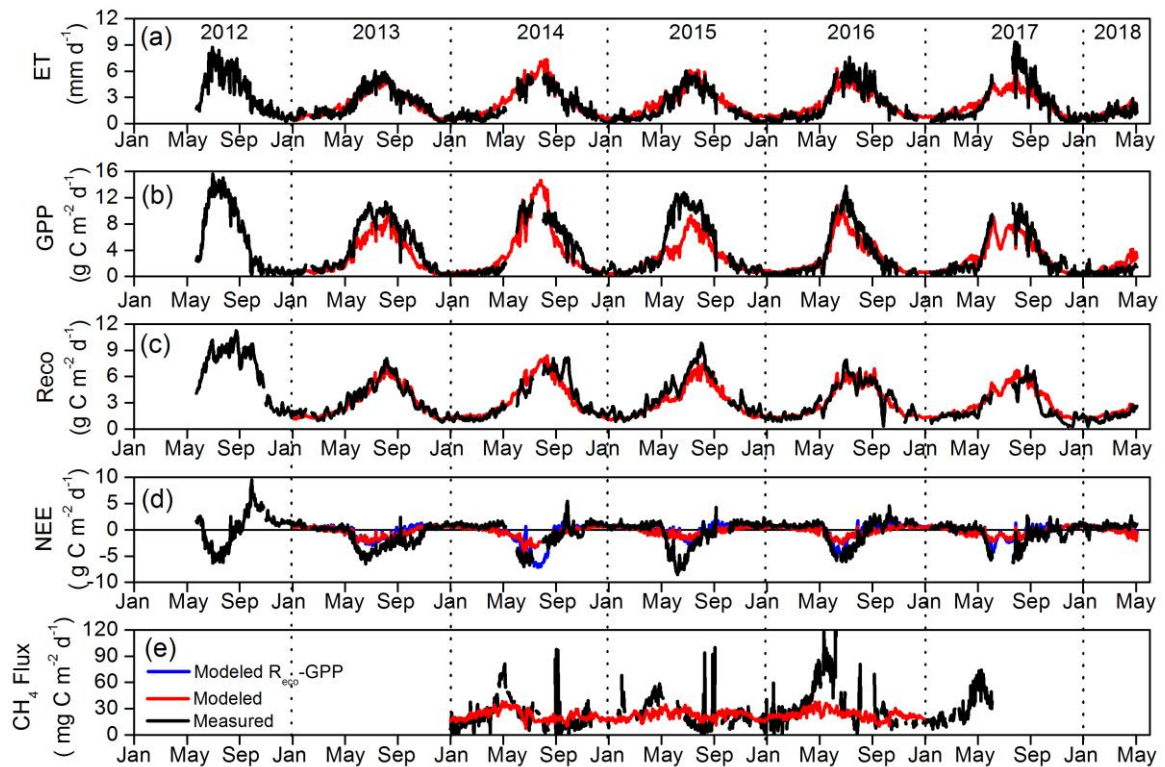
Figure 9. Daily values of measured and modeled (a) evapotranspiration (ET), (b) gross primary production (GPP), (c) ecosystem respiration (R_{eco}), (d) net ecosystem CO_2 exchange (NEE) and (e) CH_4 fluxes. Measured values are in black color and modeled values using multiple linear regression are in red (MLR model), additionally modeled NEE as modeled R_{eco}-modeled GPP is presented in blue color.

Relationships between annual averages of possible controlling factors and C fluxes and ET were found, despite the relatively low number of years (5 for CO_2 fluxes and ET and 3 for CH_4 flux). Annual values of ET and R_{eco} appeared to be correlated with the annual averaged GWL (p-values= 0.03 and 0.06 respectively), whereas NEE and CH_4 flux were correlated with the number of days of C uptake and the number of days with water table below the surface, respectively (p-values= 0.03 and 0.06 respectively).

5 Discussion

The present study, based on a robust database (6 years for CO_2 and ET fluxes and 3 years for CH_4 fluxes), provides relevant information about seasonal and interannual variability of carbon and ET fluxes in Mediterranean reed wetlands together with their possible drivers. In this regard, our results consolidate some patterns already predicted and measured in previous studies about GHG fluxes in reed wetlands, such as the great variability at seasonal scale linked to growth dynamics of reeds [*Han et al.*, 2013; *Sung-Ching et al.*, 2015; *Zhang et al.*, 2016]. But also, this study presents the first results of interannual variability of carbon and ET fluxes in Mediterranean reed wetlands together with the contribution of CH_4 fluxes into the annual budget of CO_2

equivalents of such reed communities characterized by seasonal flooding. In this section, we will discuss the most relevant and controversial results.

The averaged annual values of ET and NEE obtained in this study are in the range of those measured previously in other reed wetlands. Regarding ET, similar to other studies at similar latitudes [*Borin et al.*, 2011; *Xu et al.*, 2011; *Zhang et al.*, 2016], we measured mean annual values of ET exceeding twice the mean annual precipitation (ET=840±90 mm y^{-1}; P=340±60 mm y^{-1}; period 2013-2017). For NEE, the averaged value measured for the 5 complete years was -260±160 gC m^{-2} y^{-1}, within the range of those reported by *van der Berg* [2016], *Zhang et al.* [2016], *Sung et al.* [2015] for reed communities in Germany, northwestern China and Taiwan, respectively. Unfortunately, the length of the database of such studies did not allow to analyze the interannual variability.

In this regard, one of the most relevant and unexpected results of our study is the great interannual variability measured for NEE, never reported before in any other wetland [*Helfter et al.*, 2015; *McVeigh et al.*, 2014] and rarely reported in other natural undisturbed ecosystem types [*D Baldocchi et al.*, 2018; *Marcolla et al.*, 2017]. The annual values of NEE in the Mediterranean wetland ranged from -10±20 g C (CO_2) m^{-2} y^{-1} in 2016 to around -410±30 g C (CO_2) m^{-2} y^{-1} just one year later (and similar values in 2013), passing through intermediate values around -230 g C (CO_2) m^{-2} y^{-1} in 2014 and 2015. Such variability (standard deviation exceeding 60% the mean annual NEE) is equivalent to those measured in broadleaf forests [*Carrara et al.*, 2004; *Gielen et al.*, 2013; *Pilegaard et al.*, 2011; *Zeri et al.*, 2014]. However, none of these studies reported annual NEE varying by more than 95% in only one year with no relevant differences in meteorological conditions detected (Table 1), which is the case of the studied reed wetland in 2016 and 2017.

Table 3. Summary of simple linear regression models fitted on annual values of water/carbon fluxes.

Response variable	Explanatory variable	β	SE	p-value	Efron´s R^2
ET	(Intercept)	781	18	<0.001	
	GWL	-730	190	0.03	0.83
R_{eco}	(Intercept)	1300	60	<0.001	
	GWL	1900	600	0.06	0.75
GPP	(Intercept)	1000	300	0.06	
	Length of C uptake	3	2	0.23	0.45
NEE	(Intercept)	330	190	0.18	
	Length of C uptake	-4.1	1.3	0.05	0.77
CH_4 flux	(Intercept)	-7.6	1.5	0.13	
	GWL below surface	0.20	0.002	0.06	0.99

Note. Evapotranspiration (ET); ecosystem respiration (R_{eco}); growth primary production (GPP); net ecosystem exchange (NEE); ground water level (GWL);, the number of days of C uptake per year (length of C uptake); the number of days with water table level below the surface per year (GWL below surface); linear regression coefficient (β); standard error of β (SE); proportion of explained variance (Efrons's R^2).Results are based on $n = 5$observations except for CH_4 model which is based on $n = 3$ observations.

The variability in the annual budget of NEE appeared to be determined by differences in the balance of photosynthesis and respiration processes mostly during the transition period (Figure 8a). Whereas the senescence and growth periods behave always as carbon source and carbon sink respectively, the transition period (from 1st

August to 14th November) switches from a carbon sink to a source depending on the year. Concretely, the imbalance seems to be most closely related to variations in GPP rather than respiration dynamics (notice the size of the standard deviation of GPP and R_{eco} in Figure 7a for the transition period). Regarding possible factors explaining such variations, our linear regression analysis suggests that EVI, as a proxy for vegetation phenology, was overall the strongest control of GPP and also contributed substantially to explain the variations in R_{eco}. Same results were found in a boreal wetland [*Järveoja et al.*, 2018]. Additionally, T_s contributed to explain daily variations of GPP and was clearly the main driver controlling R_{eco}. In order to provide information about the underlying mechanisms producing the fluxes [*Pinheiro and Bates*, 2000], we applied non linear regressions using the main controlling factor determined by the MLR models for each flux. Such analisys determined that GPP and ET increased via simple logistic functions with EVI and T_s respectively (Figure 10; Table 4), whereas R_{eco} increased exponentially because of increased T_s (Figure 10) following the van't Hoff equation [*Davison et al.*, 2006] and obtaining a temperature sensibility (Q10) of 4.5 (Figure 10; Table 4). The good agreement between the modeled and measured fluxes allows us to attribute the behavior of these fluxes to typical biological growth processes [*Turchin*, 2001]. However, since half-hourly R_{eco} values were estimated from NEE, measurements may include spurious correlation with T_s and its result for R_{eco} should be taken with caution. allowed us together with a physical interpretation of their parameters.

Table 4. Summary of non-linear models fitted on daily average values of carbon/water fluxes.

Carbon/water flux	Controlling factor	Parameter	Estimate	SE
ET*[1]	T_s	φ_1	5.8	0.4
		φ_2	12.4	0.4
		φ_3	2.6	0.2
GPP*[1]	EVI	φ_1	10.3	0.6
		φ_2	0.383	0.008
		φ_3	0.064	0.006
R_{eco}*[2]	T_s	α	0.52	0.05
		β	0.152	0.005

Notes: Evapotranspiration (ET); growth primary production (GPP); ecosystem respiration (R_{eco}); soil temperature (T_s); enhanced vegetation index (EVI). φ_n are the fitted parameters of the simple logistic model $(y=\varphi_1/(1+exp((\varphi_2-x)/\varphi_3))$, with φ_1, the horizontal asymptote as the controlling variable $x\rightarrow\infty$; φ_2, the x value at the inflection point of the sigmoid (the value of x for which the response variable $y = \varphi_1/2$); and φ_3, a scale parameter on the x-axis. α and β are the fitted parameters of the van´t Hoff´s exponential model $(y= \alpha*exp(\beta*x)$, α is the respiration rate at 0ºC and β a temperature-response coefficient related to Q10 as $Q_{10} = e^{\beta x10}$; SE is the standard error of parameters. Models were fitted by non-linear generalized least squares. The serial correlation was modeled with an autoregressive-moving-average process (ARMA(p, q), with p and q the orders of the autoregressive and moving-average parts, respectively). In the ET model, the residual variance was modeled as a power of the fitted values. After these procedures, all models assumptions (normality, homoscedasticity and independence of residuals) were reasonable. Results are based on $n = 2177$ observations; p-value for all parameters <0.0001.
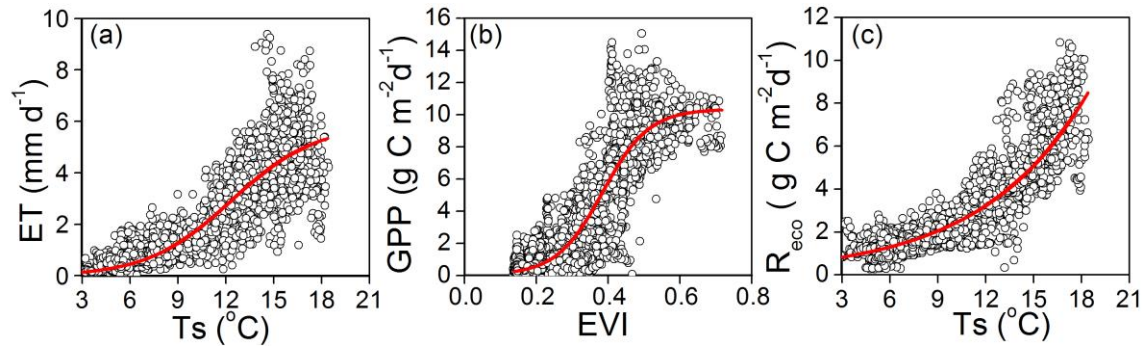
Figure 10. Daily values of (a) evapotranspiration (ET), (b) gross primary production (GPP) and (c) ecosystem respiration (R_{eco}) plotted has a function of Ts, EVI and Ts respectively.

Additionally, annual values of NEE, as found by other researchers, were significantly correlated to the length of the season with C uptake [*Helfter et al.*, 2015; *McVeigh et al.*, 2014] (Table 3). Additionally, annual values of R_{eco} appear to increase for years with a higher GWL average (Table 3; p-value=0.06). Such a result can be associated with an increase of CH_4 formation due to anoxic conditions that can be rapidly oxidize to CO_2 and emitted to the atmosphere when the soil dries. However, since we only have five complete years of measurements and the range of the measured values of some controlling factors is very limited, we should view such tendencies with caution. Increasing the sample size with more years of observations is necessary to confirm the effect of the controlling factors selected by annual models due to p-values close to the 5% significance level.

Regarding CH_4 emissions, annual values measured in the Mediterranean wetland (ranging from 9 gC(CH_4) m^{-2} y^{-1} in 2014 and 2015 to 12 gC(CH_4) m^{-2} y^{-1} in 2016) fall within the range of other natural wetlands in artic, boreal and temperate regions [*Petrescu et al.*, 2015] but are around three times lower than those reported by *Zhang et al.* [2016] for a Chinese reed. The great variability in the GWL (including periods with GWL below the surface), may have inhibited CH_4 production, and even promoted CH_4 oxidation for certain periods. What is more, reestablishment of microbial communities after prolonged drying can be very slow [*Juottonen et al.*, 2012]. Additionally, the area selected for the eddy covariance measurements is mainly composed of sand and gravel intercalated with peat, such soil properties may limit the development of a methanogenic community or even contain iron concentrations inhibiting CH_4 fluxes [*Chamberlain et al.*, 2018]. Incubation experiments of anaerobic substrate samples taken from the eddy covariance tower footprint, reported CH_4 production ranging from 1% (at 5ºC) to 8% (at 25ºC) of the total gas production (CO_2 + CH_4) [*Bockermann*, 2013]. However, despite its low contribution to the annual budget (from 2 to 5 % of the total CO_2-eq), our study showed that in years like 2016, when NEE was largely reduced, CH_4 emissions were much larger, transforming the ecosystem from a GHG sink into a source.

Similar to other studies in wetlands [*Pugh et al.*, 2018], greater soil temperature and GWL appear to increase daily CH_4 emissions in the Mediterranean reed wetland, whereas EVI is negatively related to CH_4 fluxes. In winter/late fall, low CH_4 fluxes were measured (values around 20 mg C d^{-1}; Figure 5c) coinciding with the lowest soil temperatures and highest values of GWL (Figure 3). As soil temperatures start to increase in the spring, an increase in CH_4 fluxes was measured (up to 100 mg C d^{-1}), but the fluxes then decreased again as water levels drop well below the soil surface in

summer and the rate of CH_4 oxidation increases [*Dalal et al.*, 2008], limiting CH_4 emissions. In this regard, the apparent negative contribution of EVI in the magnitude of daily CH_4 emissions appeared to be a result of the asynchronous patterns between GWL and EVI daily values, with maximum values of EVI coinciding with minimum values of GWL inhibiting CH_4 production. Furthermore, the peak of CH_4 emissions occurring in May for all study years, suggests that not only the presence of water layer (anoxic conditions) was required for CH_4 emissions but also common reed production. In any case, given the great variety of factors affecting CH_4 production – such as temperature, pH, primary production, aeration, substrate, peat chemical characteristics, and groundwater level [*Dalal et al.*, 2008] –, more research is needed in order to understand the magnitude and timing of their effects [*Sturtevant et al.*, 2015].

As expected, despite the low magnitude of CH_4 fluxes compared to other reeds, the transport of CH_4 trough the reeds appears to control the daily patterns. Different studies have concluded that more than 80% of the total emissions of CH_4 from soil to the atmosphere occurs through the aerenchyma of reeds and other wetland plants [*Cheng et al.*, 2006; *Dacey and Klug*, 1979; *Kreuzwieser et al.*, 2003]. In this regard, as expected, the diurnal variations in CH_4 emission of our study sites followed the diurnal valley-peak pattern during both seasons (Figure 5). Additionally, similar to other studies [*Chanton et al.*, 1993], half hourly CH_4 emissions were correlated with PPFD (r=0.65; n=1640) and peaked in the early daylight hours during the early growing season. Such a relation was not observed for the rest of the year. This pattern can be explained by stomata opening and the increasing solar illumination driving pressurized bulk flow through the plant [*Armstrong and Armstrong*, 1988; *Dacey*, 1981], with fluxes tailing off due to depletion of CH_4 that had accumulated during the night.

6 Conclusions

This study is the first to quantify the interannual variability of carbon (CO_2 and CH_4) and ET in a Mediterranean reed wetland with seasonal flooding . Our results show an unexpected great interannual variability in the annual budget of CO_2 equivalents ranging from a CO_2 sink of -660±150 g CO_2-eq m^{-2} in 2014 to a source of 360±120 gCO_2-eq m^{-2} in 2016. Such variability appeared to be mostly dominated by variations of reed growth from August to mid-November (transition period). Such production (daily values of GPP) seemed mainly be explained by soil temperature and patent in the greenness index derived from digital images (EVI). Regarding evapotranspiration processes, its daily variability was mainly explained by soil temperature but, contrary to expected, its interannual variability was not remarkable. Additionally, the GHG budget (CO_2-eq) measured in 2016 revealed the relative relevance of CH_4 emissions, which, in spite of being lower than in other studied wetlands, determined the mitigation capacity of our reed wetland, transforming this ecosystem from a GHG sink to a source when the measured annual NEE were close to neutral values. To conclude, our findings reveal the great vulnerability of the annual GHG sink capacity of Mediterranean reed wetlands to changes in soil temperature and greenness index, occurring mainly in late summer and autumn.

References

Anthony, K. W., and S. MacIntyre (2016), Nocturnal escape route for marsh gas, *Nature*, *535*, 363.

Armstrong, J., and W. Armstrong (1988), Phragmites australis– A preliminary study of soil-oxidizing sites and internal gas transport pathways, *New Phytologist*, *108*(4), 373-382.

Arya, S. P. (1988), *Introduction to micrometeorology*, 307 pp., Academic Press, London.

Baldocchi, D. (2014), Measuring fluxes of trace gases and energy between ecosystems and the atmosphere – the state and future of the eddy covariance method, *Global Change Biology*, *20*(12), 3600-3609.

Baldocchi, D., H. Chu, and M. Reichstein (2018), Inter-annual variability of net and gross ecosystem carbon fluxes: A review, *Agricultural and Forest Meteorology*, *249*, 520-533.

Baldocchi, D. D., et al. (2001), FLUXNET: A new tool to study the temporal and spatial variability of ecosystem-scale carbon dioxide, water vapor, and energy flux densities, *Bulletin of the American Meteorological Society*, *82*, 2415–2434.

Bockermann, C. (2013), Potential temperature-induced changes in soil organic matter in a Mediterranean wetland, Southern Spain, MSc Thesis for the School of Integrated Climate System Sciences, University of Hamburg, Germany.

Borin, M., M. Milani, M. Salvato, and A. Toscano (2011), Evaluation of Phragmites australis (Cav.) Trin. evapotranspiration in Northern and Southern Italy, *Ecological Engineering*, *37*(5), 721-728.

Breiman, L. (1996), Bagging Predictors, *Machine Learning*, *24*(2), 123-140.

Breiman, L. (2001), Random Forests, *Machine Learning*, *45*(1), 5-32.

Brix, H., B. K. Sorrell, and B. Lorenzen (2001), Are Phragmites-dominated wetlands a net source or net sink of greenhouse gases? , *Aquatic Botany*, 69, 313-324.

Carrara, A., I. A. Janssens, J. C. Yuste, and R. Ceulemans (2004), Seasonal changes in photosynthesis, respiration and NEE of a mixed temperate forest, *Agricultural and Forest Meteorology*, *126*, 15-31.

Chamberlain, S. D., T. L. Anthony, W. L. Silver, E. Eichelmann, K. S. Hemes, P. Y. Oikawa, C. Sturtevant, D. J. Szutu, J. G. Verfaillie, and D. D. Baldocchi (2018), Soil properties and sediment accretion modulate methane fluxes from restored wetlands, *Global Change Biology*, *24*(9), 4107-4121.

Chanton, J. P., G. J. Whiting, J. D. Happell, and G. Gerard (1993), Contrasting rates and diurnal patterns of methane emission from emergent aquatic macrophytes, *Aquatic Botany*, *46*(2), 111-128.

Chatterjee, S., and A. S. Hadi (2012), Regression analysis by example.

Cheng, W., K. Yagi, H. Sakai, and K. Kobayashi (2006), Effects of Elevated Atmospheric CO2 Concentrations on CH4 and N2O Emission from Rice Soil: An Experiment in Controlled-environment Chambers, *Biogeochemistry*, *77*(3), 351-373.

Clevering, O. A., and J. Lissner (1999), Taxonomy, chromosome numbers, clonal diversity and population dynamics of Phragmites australis, *Aquatic Botanic*, *64*, 185-208.

Crundwell, M. E. (1986), A review of hydrophyte evapotranspiration, *Revue d'Hydrobiologie Tropicale*, *19*(3-4), 215-232.

Dabberdt, W. F., D. H. Lenschow, T. W. Horst, P. R. Zimmerman, S. P. Oncley, and A. C. Delany (1993), Atmosphere-surface exchange measurements, *Science*, *260*, 1472-1481.

Dacey, J. W. H. (1981), Pressurized Ventilation in the Yellow Waterlily, *Ecology*, *62*(5), 1137-1147.

Dacey, J. W. H., and M. J. Klug (1979), Methane efflux from lake sediments through water lilies, *Science*, *203*, 1253 - 1255.

Dalal, R. C., D. E. Allen, S. J. Livesley, and G. Richards (2008), Magnitude and biophysical regulators of methane emission and consumption in the Australian agricultural, forest, and submerged landscapes: a review, *Plant and Soil*, *309*(1-2), 43-76.

Davidson, E. A., I. A. Janssens, and Y. Luo (2006), On the variability of respiration in terrestrial ecosystems: moving beyond Q10, *Global Change Biology, 12*(2), 154-164.

Didan, K. (2015), MOD13Q1 MODIS/Terra Vegetation Indices 16-Day L3 Global 250m SIN Grid V006. NASA EOSDIS Land Processes DAAC. https://doi.org/10.5067/MODIS/MOD13Q1.006.

Engloner, A. I. (2009), Structure, growth dynamics and biomass of reed (Phragmites australis) – A review, *Flora*, *204*, 331-346.

Gielen, B., B. De Vos, M. Campioli, J. Neirynck, D. Papale, A. Verstraeten, R. Ceulemans, and I. A. Janssens (2013), Biometric and eddy covariance-based assessment of decadal carbon sequestration of a temperate Scots pine forest, *Agricultural and Forest Meteorology*, *174-175*, 135-143.

Han, G., L. Yang, J. Yu, G. Wang, P. Mao, and Y. Gao (2013), Environmental Controls on Net Ecosystem CO2 Exchange Over a Reed (Phragmites australis) Wetland in the Yellow River Delta, China, *Estuaries and Coasts*, *36*(2), 401-413.

Helfter, C., C. Campbell, K. J. Dinsmore, J. Drewer, M. Coyle, M. Anderson, U. Skiba, E. Nemitz, M. F. Billett, and M. A. Sutton (2015), Drivers of long-term variability in CO_2 net ecosystem exchange in a temperate peatland, *Biogeosciences*, *12*(6), 1799-1811.

Huete, A., K. Didan, T. Miura, E. P. Rodriguez, X. Gao, and L. G. Ferreira (2002), Overview of the radiometric and biophysical performance of the MODIS vegetation indices, *Remote Sensing of Environment*, *83*, 195-213, doi:110.1016/S0034-4257(1002)00096-00092.

IPCC (2013), Climate Change 2013: The Physical Science Basis. Contribution of Working Group I to the Fifth Assessment Report of the Intergovernmental Panel on Climate Change, edited, Cambridge University Press.

Janssens, I. A., et al. (2003), Europe's Terrestrial Biosphere Absorbs 7 to 12% of European Anthropogenic CO2 Emissions, *Science*, *300*, 1538-1542.

Järveoja, J., M. B. Nilsson, M. Gažovič, P. M. Crill, and M. Peichl (2018), Partitioning of the net CO2 exchange using an automated chamber system reveals plant phenology as key control of production and respiration fluxes in a boreal peatland, *Global Change Biology*, *24*(8), 3436-3451.

Juottonen, H., A. Hynninen, M. Nieminen, T. T. Tuomivirta, E.-S. Tuittila, H. Nousiainen, D. K. Kell, K. Yrjälä, A. Tervahauta, and H. Fritze (2012), Methane-Cycling Microbial Communities and Methane Emission in Natural and Restored Peatlands, *Applied and Environmental Microbiology*, *78*(17), 6386-6389.

Keeling, C. D. (1960), The concentration and isotopic abundance of carbon dioxide in the atmosphere., *Tellus*, *12*, 200-203.

Kim, J., S. B. Verma, D. P. Billesbach, and R. J. Clement (1998), Diel variation in methane emission from a midlatitude prairie wetland: Significance of convective throughflow in Phragmites australis, *Journal of Geophysical Research: Atmospheres*, *103*(D21), 28029-28039.

Kirschke, S., et al. (2013), Three decades of global methane sources and sinks, *Nature Geosci*, *6*(10), 813-823.

Kljun, N., P. Calanca, M. W. Rotach, and H. P. Schmid (2004), A Simple paraemeterisation por flux footprint predictions, *Boundary-Layer Meteorology*, *112*, 503-523.

Kowalski, A. S., P. M. Anthoni, and R. J. Vong (1997), Deployment and Evaluation of a System for Ground-Based Measurement of Cloud Liquid Water Turbulent Fluxes, *Journal of atmospheric and oceanic technology*, *14*, 468-479.

Kreuzwieser, J., J. Buchholz, and H. Rennenberg (2003), Emission of Methane and Nitrous Oxide by Australian Mangrove Ecosystems, *Plant biology*, *5*(4), 423-431.

Luo, Y. (2007), Terrestrial Carbon–Cycle Feedback to Climate Warming, *Annual Review of Ecology, Evolution, and Systematics*, *38*, 683-712.

Marcolla, B., C. Rödenbeck, and A. Cescatti (2017), Patterns and controls of inter-annual variability in the terrestrial carbon budget, *Biogeosciences*, *14*(16), 3815-3829.

Mauder, M., and T. Foken (2004), *Documentation and Instruction Manual of the Eddy-Covariance Software Package TK3*, Universität Bayreuth, Abteilung Mikrometeorologie ed., Foken, T.

McVeigh, P., M. Sottocornola, N. Foley, P. Leahy, and G. Kiely (2014), Meteorological and functional response partitioning to explain interannual variability of CO2 exchange at an Irish Atlantic blanket bog, *Agricultural and Forest Meteorology*, *194*, 8-19.

Millennium-Ecosystem-Assessment (2005), *Ecosystems and Human Well-being: Wetlands and Water Synthesis.* , Washington, D. C.

Moncrieff, J. B., J. M. Massheder, H. Bruin, J. Elbers, T. Friborg, H. b. B., P. Kabat, S. Scott, H. Soegaard, and A. Verhoef (1997), A system to measure surface fluxes of momentum, sensible heat, water vapour and carbon dioxide, *Journal of Hydrology*, *188-189*, 589-611.

Moncrieff, J. B., R. Clement, J. Finnigan, and T. Meyers (2004), Averaging, detrending and filtering of eddy covariance time series, in Handbook of micrometeorology: a guide for surface flux measurements.

Moro, M. J., F. Domingo, and G. López (2004), Seasonal transpiration pattern of Phragmites australis in a wetland of semi-arid Spain, *Hydrological Processes*, *18*(2), 213-227.

ORNL DAAC, (2018), MODIS and VIIRS Land Products Global Subsetting and Visualization Tool. ORNL DAAC, Oak Ridge, Tennessee, USA. Accessed September 18, 2018. Subset obtained for MOD13Q1 product at 37.0117N,3.6068W, time period: 2012-01-01 to 2018-08-13, and subset size: 0.25 x 0.25 km. https://doi.org/10.3334/ORNLDAAC/1379.

Ortiz, J. E., T. Torres, A. Delgado, R. Julia, M. Lucini, F. J. Llamas, E. Reyes, V. Soler, and M. Valle (2004), The palaeoenvironmental and palaeohydrological evolution of Padul Peat Bog (Granada, Spain) over one million years, from elemental, isotopic and molecular organic geochemical proxies, *Organic Geochemistry*, *35*, 1243-1260.

Papale, D., et al. (2006), Towards a standardized processing of Net Ecosystem Exchange measured with eddy covariance technique: algorithms and uncertainty estimation, *Biogeosciences*, *3*, 571–583.

Petrescu, A. M. R., et al. (2015), The uncertain climate footprint of wetlands under human pressure, *Proceedings of the National Academy of Sciences*, *112*(15), 4594-4599.

Pilegaard, K., A. Ibrom, M. S. Courtney, P. Hummelshøj, and N. O. Jensen (2011), Increasing net CO2 uptake by a Danish beech forest during the period from 1996 to 2009, *Agricultural and Forest Meteorology*, *151*(7), 934-946.

Pinheiro, J. C., and D. M. Bates (2000), Mixed-effects models in S and S-Plus.

Pugh, C. A., D. E. Reed, A. R. Desai, and B. N. Sulman (2018), Wetland flux controls: how does interacting water table levels and temperature influence carbon dioxide and methane fluxes in northern Wisconsin?, *Biogeochemistry*, *137*(1), 15-25.

R Core Team (2019). R: A Language and Environment for StatisticalComputing. R foundation for Statistical Computing, Vienna, URL https://www.r-project.org/.

Raddatz, R. L., T. N. Papakyriakou, K. A. Swystun, and M. Tenuta (2009), Evapotranspiration from a wetland tundra sedge fen: Surface resistance of peat for land-surface schemes, *Agricultural and Forest Meteorology*, *149*(5), 851-861.

Reichstein, M., et al. (2005), On the separation of net ecosystem exchange into assimilation and ecosystem respiration: review and improved algorithm, *Global Change Biology*, *11*, 1-16.

Saunois, M., R. B. Jackson, P. Bousquet, B. Poulter, and J. G. Canadell (2016a), The growing role of methane in anthropogenic climate change, *Environmental Research Letters*, *11*(12), 120207.

Saunois, M., et al. (2016b), The global methane budget 2000–2012, *Earth Syst. Sci. Data*, *8*(2), 697-751.

Stoy, P., et al. (2013), A data-driven analysis of energy balance closure across FLUXNET research sites: The role of landscape-scale heterogeneity, *Agricultural and Forest Meteorology*, *171-172*, 137-152.

Sturtevant, C., B. L. Ruddell, S. H. Knox, J. Verfaillie, J. H. Matthes, P. Y. Oikawa, and D. Baldocchi (2015), Identifying scale-emergent, non-linear, asynchronous processes of wetland methane exchange, *Journal of Geophysical Research: Biogeosciences*, *120*, doi:10.1002/2015JG0030054.

Sung-Ching, L., F. Chao-Jung, W. Zih-Yi, and J. Jehn-Yih (2015), Investigating effect of environmental controls on dynamics of CO 2 budget in a subtropical estuarial marsh wetland ecosystem, *Environmental Research Letters*, *10*(2), 025005.

Turchin, P. (2001), Does population ecology have general laws?, *Oikos, 94*(1), 17-26.

Valentini, R., et al. (2000), Respiration as the main determinant of carbon balance in European forests, *Nature*, *404*, 861 - 865.

Webb, E. K., G. I. Pearman, and R. Leuning (1980), Correction of flux measurements for density effects due to heat and water vapour transfer, *Quarterly Journal of the Royal Meteorological Society*, *106*(447), 85-100.

Wilson, K., et al. (2002), Energy balance closure at FLUXNET sites, *Agricultural and Forest Meteorology*, *113*(1–4), 223-243.

Xu, S., T. Ma, and Y. Liu (2011), Application of a multi-cylinder evapotranspirometer method for evapotranspiration measurements in wetlands, *Aquatic Botany*, *95*(1), 45-50.

Zeri, M., L. D. A. Sá, A. O. Manzi, A. C. Araújo, R. G. Aguiar, C. von Randow, G. Sampaio, F. L. Cardoso, and C. A. Nobre (2014), Variability of Carbon and Water Fluxes Following Climate Extremes over a Tropical Forest in Southwestern Amazonia, *PLOS ONE*, *9*(2), e88130.

Zhang, Q., R. Sun, G. Jiang, Z. Xu, and S. Liu (2016), Carbon and energy flux from a Phragmites australis wetland in Zhangye oasis-desert area, China, *Agricultural and Forest Meteorology*.

Zuur, A., Ieno, E. N., Walker, N., Saveliev, A. A., and G. M. Smith (2009). Mixed effects models and extensions in ecology with R. Springer Science & Business Media.